Published paper

Research Paper

Electrospun polyurethane/hydroxyapatite bioactive Scaffolds for bone tissue engineering: The role of solvent and hydroxyapatite particles ☆

CrossMark

G. Tetteh, A.S. Khan[1], R.M. Delaine-Smith[2,3], G.C. Reilly*, I.U. Rehman

Kroto Research Institute, Department of Materials Science and Engineering, University of Sheffield, Sheffield S3 7HQ, UK

ARTICLE INFO

ABSTRACT

Polyurethane (PU) is a promising polymer to support bone–matrix producing cells due to its durability and mechanical resistance. In this study two types of medical grade poly-ether urethanes Z3A1 and Z9A1 and PU-Hydroxyapatite (PU–HA) composites were investigated for their ability to act as a scaffold for tissue engineered bone. PU dissolved in varying concentrations of dimethylformamide (DMF) and tetrahydrofuran (THF) solvents were electrospun to attain scaffolds with randomly orientated non-woven fibres.

Bioactive polymeric composite scaffolds were created using 15 wt% Z3A1 in a 70/30 DMF/THF PU solution and incorporating micro- or nano-sized HA particles in a ratio of 3:1 respectively, whilst a 25 wt% Z9A1 PU solution was doped in ratio of 5:1. Chemical properties of the resulting composites were evaluated by FTIR and physical properties by SEM. Tensile mechanical testing was carried out on all electrospun scaffolds. MLO-A5 osteoblastic mouse cells and human embryonic mesenchymal progenitor cells, hES-MPs were seeded on the scaffolds to test their biocompatibility and ability to support mineralised matrix production over a 28 day culture period. Cell viability was assayed by MTT and calcium and collagen deposition by Sirius red and alizarin red respectively.

SEM images of both electrospun PU scaffolds and PU–HA composite scaffolds showed differences in fibre morphology with changes in solvent combinations and size of HA particles. Inclusion of THF eliminated the presence of beads in fibres that were present in scaffolds fabricated with 100% DMF solvent, and resulted in fibres with a more uniform morphology and thicker diameters. Mechanical testing demonstrated that the Young's Modulus and yield strength was lower at higher THF concentrations. Inclusion of both sizes of HA particles in PU–HA solutions reinforced the scaffolds leading to higher mechanical properties, whilst FTIR characterisation confirmed the presence of HA in all composite scaffolds.

Although all scaffolds supported proliferation of both cell types and deposition of calcified matrix, PU–HA composite fibres containing nano-HA enabled the highest cell viability and collagen deposition. These scaffolds have the potential to support bone matrix formation for bone tissue engineering.

1. Introduction

Bone tissue engineering aims at improving musculoskeletal health by providing a living bone graft substitute to fill and aid in the repair of bone defects caused by trauma, disease, or congenital malformations or to augment bone stock around an implant site. While small bone defects heal spontaneously, critical size defects do not heal during a lifetime (Gogolewski and Gorna, 2007). Bone tissue engineering involves the use of materials to either induce formation of bone from the surrounding tissue or to act as a carrier or template for implanted bone cells. Bone regeneration requires four components: a morphogenetic signal, responsive host cells, a suitable carrier to serve as scaffolding for the growth of host cells and a viable and well vascularised host bed (Croteau et al., 1999; Burg et al., 2000). The scaffold provides a three dimensional porous structure that facilitates cell attachment, growth and matrix deposition.

Orthopaedic implant materials were initially selected for structural restoration based on their biomechanical properties (termed 'first generation implants'). Later bone implant materials were engineered to be bioactive or bioresorbable to enhance tissue growth ('second generation'), a development which coincided with the development of tissue engineering scaffolds as cell supports for multiple tissue types. Currently, bone implant materials are designed to induce bone formation (Bose et al., 2012) and many bone graft substitute materials are also used as experimental scaffolds to support cells for bone tissue engineering.

An ideal scaffold should possess a suitable surface chemistry that supports cell attachment, proliferation, migration and growth. Additionally, it should serve as a biocompatible template for osteoprogenitor cell growth and aid in the differentiation of mesenchymal stem cells into osteoblasts, as well as supporting the production, organisation and maintenance of an extracellular matrix (Gogolewski, 2007; Gorna and Gogolewski, 2003). In addition to being biocompatible, scaffolds are required to be composed of highly interconnected macro and micro-porous networks to facilitate cell migration and nutrient distribution.

Several polymers of both natural and synthetic origin can be used for bone tissue engineering; however polyurethanes are of particular interest due to the flexibility associated with their versatile chemistry (Guelcher, 2008). This makes it possible to customise scaffolds in order to attain desirable chemical, physical and mechanical properties such as durability, elasticity and fatigue resistance, by altering the choice and quantity of the starting materials (Zdrahala and Zdrahala, 1999). Biocompatible and biodegradable polyurethanes have been investigated as scaffolds for tissue engineering applications for almost thirty years (Guelcher et al., 2004), and also as heart valves, stents, intra-aortic balloons and pacing lead insulators, amongst others (Grad et al., 2003).

The microphase separation between the hard and soft segments enables polyurethane to withstand physical stresses and therefore it possesses desirable mechanical properties useful for dynamic bone tissue engineering (Wen et al., 1997). For example, we have demonstrated that cyclic mechanical conditioning of osteoprogenitor cells in a PU scaffold upregulates bone formation (Sittichockechaiwut et al., 2009; Sittichockechaiwut et al., 2010; Delaine-Smith and Reilly, 2011). PU has several advantages as a scaffold for cells that will be subjected to mechanical conditioning, as its high yield strain and fatigue life enable it to undergo repeated cycles of mechanical strain, without changing its mechanical properties. Additionally, the use of elastomeric scaffolds as alternatives to bone grafts, prevents generation of shear forces at the interface between native bone and the substitute; thus enhancing intimate contact with bone and enabling the proliferation of osteogenic cells and bone regeneration (Gorna and Gogolewski, 2003).

Composite scaffolds range from stable to degradable, and most of those used in tissue engineering/regenerative medicine are biodegradable polymers reinforced with ceramic particles. Bonfield first proposed the concept of polymer–ceramic combination materials, mimicking the ductile and brittle properties of the collagen and mineral components of bone respectively, in 1988, which was later commercialised with the trade name, HAPEX™ (Bonfield, 1988a, 1988b). Mechanically, polymers are noted for their extensive deformation and high toughness whilst ceramics, such as hydroxyapatites (HA), are noted for their high compressive strength but brittle failure. Combining polyurethane with hydroxyapatite has been shown by a number of researchers to improve the mechanical properties of the resulting composite, as long as a strong interfacial bond strength is established between the ceramic phase and the polymer matrix (Attawia et al., 1995; Boccaccini and Maquet, 2003; Bonzani et al., 2007; Martinez-Valencia et al., 2011).

Previous research has been undertaken on the synthesis of PU with varying additives such as ascorbic acid (Zhang et al., 2003) HA (Gorna and Gogolewski, 2003), and β-tri-calcium phosphate (Adhikari et al., 2008; Yoshii et al., 2012). Others have investigated fabrication techniques for PU scaffolds including Thermally Induced Phase Separation (TIPS) (Tsui and Gogolewski, 2009) and Solvent Casting/Particulate Leaching (Gorna and Gogolewski, 2006; Heijkants et al., 2006; Kucinska-Lipka et al., 2013; Boissard et al., 2009). However, to date little work has been undertaken on electrospinning of

polyurethane composites for bone tissue engineering applications.

Electrospinning is an efficient, simple and relatively easy polymer fabrication technique that produces nano and micro diameter polymer fibres, with the advantage that it can be performed with different polymers in both solution and melt states. Such thin fibres provide high surface area to volume ratios, high porosity, flexibility in surface functionalities, superior mechanical performance and membrane technology (Demir et al., 2002). In the field of biomaterials and tissue engineering, electrospinning has been utilised for producing scaffolds that mimic the morphological characteristics and biological function of the natural extracellular matrix, by providing an optimal template for cell attachment, proliferation and growth (Carlberg et al., 2009; Huang et al., 2003). Several different polymers such as polyurethanes, poly(ε -caprolactone), poly(lactic acid), poly(glycolic acid) and their co-polymers have been successfully spun for musculoskeletal, nerve, skin, vascular and drug delivery applications (Bashur et al., 2009; Clarke et al., 2008; Nirmala et al., 2011). Electrospinning may be an ideal technique for bone tissue engineering where repair of a thin defect is required, for example a cleft palate repair (Bye et al., 2013), or electrospun sheets may be layered or rolled for larger defects (McMahon et al., 2011).

Demir et al. (2002) studied the effect of electrical field, temperature and conductivity on electrospun polyurethane–urea fibres and reported that the morphology of electrospun fibres is strongly correlated with viscosity, equivalent concentration and temperature. In their study, they reported that solution temperature, a key parameter that affects fibre morphology and spinning ability was essential to spin polymer concentrations beyond 12.8 wt%. Khan et al. (2008) and Mi et al. (2014) electrospun polyurethane composites with micro and nano sized hydroxyapatite for dental and bone tissue engineering applications, respectively. In their studies, Khan et al. developed a novel composite material by chemically binding the HA particles to the diisocyanate component of the polyurethane backbone through solvent polymerisation, whilst Mi et al. studied the effect of polymer properties and particle size on electrospun PU–HA scaffold and reported reduced tensile properties with the inclusion of micro HA

(mHA) and nano HA (nHA) particles, although the reduction was more significant with the inclusion of mHA.

The aim of this study was to identify polyurethane solutions that would create consistent microfibrous mats without beads and irregularities at room temperature and to examine the effect of incorporating HA particles into these scaffolds. Our hypothesis was that HA would reinforce the mechanical properties of polymers and improve the bioactive properties compared to polymer-only scaffolds. Our long-term aim is to create a range of scaffolds supportive of bone cell and matrix growth that can withstand mechanical conditioning *in vitro* and mechanical loading *in vivo*. In this study, we investigated the effect of dimethylformamide (DMF) and tetrahydrofuran (THF) solvent combinations on the fibre morphology and mechanical properties of electrospun thermoplastic polyether-urethane polymers Z3A1 and Z9A1. We also investigated the effect of including nano and micro size HA particles on fibre morphology, mechanical properties, biocompatibility, extracellular and calcified matrix production over a 28 day period using MLO-A5 osteoblastic mouse cells and human embryonic mesenchymal progenitor cells (hES-MPs).

2.   Materials and methods

2.1.   Polyurethane (PU) solutions

Two aromatic medical grade polyether–urethanes Z3A1 (Mn—143,566 Mw—272,857) and Z9A1 (Mn—100K_D Mw—197K_D), composed of 4,4′-diphenylmethane diisocyanate, polyether diol, and 1,4 Butane diol were obtained from Biomer Technology, UK and dissolved in dimethylformamide (DMF) and Tetrahydrofuran (THF) solvents (Sigma Aldrich, UK). 15 wt% Z3A1 pellets or 27% Z9A1 pellets were dissolved in 100% DMF, 70/30 DMF/THF (v/v) or 50/50 (v/v) DMF/THF. These solutions will be denoted as Z3-100, Z3-70, Z3-50, Z9-100, Z9-70, and Z9-50 respectively (Table 1).

2.2.   PU–HA composite solutions

For composite scaffolds, 15 wt% Z3A1 in 70/30 DMF/THF (Z3-PU) PU solutions were doped with either sintered micro HA ($<5\,\mu m$, Captal® S, Plasma Biotal, UK) or nano-sized HA

Table 1 – Parameters used in preparing electrospun scaffolds.

Name	PU (wt%)	HA (wt%)	Volumetric ratio of DMF (%)	Volumetric ratio of THF (%)	Spin speed (rpm)	Diameter of rotating drum (cm)
Z9-100	27	0	100	0	150	6
Z9-70	27	0	70	30	150	6
Z9-50	27	0	50	50	150	6
Z3-100	15	0	100	0	150	6
Z3-70	15	0	70	30	150	6
Z3-50	15	0	50	50	150	6
Z9-PU	25	0	70	30	150	6
Z9-mHA	25	5	70	30	150	6
Z9-nHA	25	5	70	30	150	6
Z3-PU	15	0	70	30	300	8
Z3-mHA	15	5	70	30	300	8
Z3-nHA	15	5	70	30	300	8

(<200 nm, Sigma Aldrich, UK) particles in a ratio of 3:1, PU: HA and will be denoted Z3-mHA or Z3-nHA, respectively (Table 1). For Z9A1 composites, 25 wt% Z9A1 in 70/30 DMF/THF (Z9-PU) was doped with HA particles in a ratio of 5:1 PU: HA and denoted as Z9-mHA and Z9-nHA. Note that this concentration of PU in the Z9A1 (no HA) group is lower than that used in the non-composite formulations described above, This is because the 27 wt% PU solutions were too viscous to enable adequate distribution of HA particles. In all preparations, solutions were stirred with magnetic beads on the UC151 ceramic plate stirrer at rotation speed of 500 rpm for 24 h at room temperature.

2.3. Electrospinning

Solutions were placed into four 5 ml syringes with 20 gauge luer stub adaptors and electrospun at a voltage of +16.5 kV, a flow rate of 3 ml/h and a tip to collector distance of 20 cm, at room temperature. A mat of randomly orientated polymeric fibres was collected on a sheet of aluminium foil wrapped around a grounded metallic mandrel, rotating at rate of 150 rpm for all scaffolds with the exception of Z3-PU, Z3-mHA and Z3-nHA which were electrospun at a rotation speed of 300 rpm. After electrospinning, the aluminium foil was removed and dried in a vacuum oven at a negative pressure of 1020 mbar for 12 h to evaporate any remaining solvent.

2.4. Scanning electron microscopy (SEM)

SEM was used to examine morphological and topographical details of electrospun scaffolds. Prior to imaging, samples were mounted onto aluminium stubs using double-sided carbon adhesive tabs (12 mm) (Agar Scientific, UK) and sputter-coated with gold powder. Coated scaffolds were imaged with secondary electrons at an accelerating voltage of 20 kV, a spot size of 3.0 and a magnification of $1250 \times$.

2.5. Mechanical testing

The mechanical properties of fabricated scaffolds were analysed in tension on a materials testing machine (ElectroForce 3200, Bose, USA). Rectangular samples with average dimensions of 5 mm $\times$ 20 mm were measured with vernier callipers, mounted between two grips to give a guage length of 6 mm and subjected to tensile strain at a rate of 1 Hz up to 100% strain. Deformation was measured by the movement of the cross-head and load measured using a 22 N load cell, the resulting load/deformation curves were converted into stress/strain curves by dividing by the sample bulk cross-sectional area. Young's modulus was calculated as change in stress divided by change in strain in the linear portion of the curve, yield was defined as the point at which the load deformation curve deviated from the straight line and yield strength was defined as the stress at yield.

2.6. Fourier transform infrared spectroscopy (FTIR)

Chemical structural characterisation of the composites was carried out using a Fourier Transform Infrared spectrometer (FTIR) (Thermo Fisher Scientific Inc., USA) equipped with a

Photo-Acoustic (PAS) sampling cell, which allows analysis of neat samples without the need for sample preparation. The PAS cell was purged with helium gas. All spectra were recorded at 4 cm^{-1} resolution, accumulating over a total of 256 scans. The spectral data was acquired and processed using the OMNIC7.4™ software.

2.7. Cell culture

All reagents were obtained from Sigma-Aldrich (UK) unless otherwise stated. Prior to cell culture, electrospun scaffolds were cut with the Epilog Mini 40 W Laser cutter (Epiloglaser, USA) with vector settings at a speed of 80% and a laser power of 6% into disks with a diameter of 1.6 cm and sterilised with 0.1% peracetic acid for 3 h at room temperature. The scaffolds were washed with PBS. Using stainless steel rings, MLO-A5 at passage 33 and hES-MP cells at passage 3 were seeded at 1.0×10^5 cells per scaffold and incubated at 37 °C in a humidified environment with 5% CO$_2$. The rings were removed after 24 h and Dulbeccos Modified Eagles Medium (DMEM) (Biosera, UK), supplemented with 10% foetal calf serum (FCS), 1% L-glutamine (L-G), 1% penicillin and streptomycin (P/S), 0.25% fungizone (F), 50 μg/ml ascorbic acid-2-phosphate and 5 mM βGP added to the scaffolds; media was changed every 2 days during the 28-day culture period. Media used for hES-MP cells was also supplemented with 100 nM of dexamethosone to stimulate osteoblastic differentiation.

2.8. MTT cell viability

MTT (3-(4, 5-dimethylthiazol-2-yl)-2, 5-diphenyltetrazolium bromide) colorimetric assay was used to investigate cell viability 1, 4, 7, 14, 21 and 28 days after seeding. For each assay, cell-seeded scaffolds were rinsed with PBS and MTT solution at 0.5 mg/ml was added to each well and incubated for a period of 40 min. The yellow MTT dye was reduced by the mitochondrial reductase enzyme in living cells to purple formazan after the incubation period; the formazan was destained with 2 ml of 0.125% acidified isopropanol and its absorbance read with the spectrophotometer at 562 nm reference 630 nm.

2.9. DAPI and phalloidin staining

Four days after cell seeding, Z3-70 and Z9-70 scaffolds seeded with MLO- A5 cells were stained with DAPI (4′, 6-diamidino-2-phenylindole dihydrochloride) nuclear stain and phalloidin fluorescent conjugate cytoskeleton stains to visualise cell attachment and cell morphology. The cells on the scaffolds were fixed with 3.7% formaldehyde for 20 min, washed with PBS and permeablized with 1% Triton X-100 in PBS. The scaffolds were then washed with PBS, 1% Bovine Serum Albumin (BSA) was added as a blocking agent and then 1% Phallodin was added. Scaffolds were then washed with PBS and stained with 0.1 μg/ml of DAPI. Finally, scaffolds were washed with PBS and visualised with a fluorescent image analyser (AXON Instruments ImageXpress 5000A, USA).

2.10. Collagen staining

Sirius red which binds to collagen was used to detect collagen at days 14, 21 and 28. The Sirius red (Direct red dye from Sigma-Aldrich, UK) solution was prepared by dissolving 1 mg/ml in saturated picric acid. Cell-seeded scaffolds were washed with PBS and fixed with 3.7% formaldehyde for 20 min, then washed with distilled water. 1 mg/ml Sirius red solution was added to each well and samples were agitated on a platform rocker at 30 rpm. After 18 h excess Sirius red solution was removed and the scaffolds washed with distilled water. Samples were allowed to air dry for 30 min and photographic images taken for qualitative analysis. For quantitative analysis, 0.2 M of NaOH and methanol at 1:1 was used to destain Sirius red on a platform rocker at 30 rpm for 24 h; the absorbance of the eluate was read with the spectrophotometer at 490 nm.

2.11. Calcium staining

Alizarin red (AR) staining was used to detect extracellular calcium deposition on days 14, 21 and 28 of culture. 1% w/v of alizarin Red S (Sigma-Aldrich, UK) powder in distilled water was used to stain MLO-A5 and hES-MPs seeded scaffolds for two hours under dynamic rocking at 30 rpm. Prior to staining, scaffolds were washed and fixed with 3.7% formaldehyde as per the procedure described for collagen staining. Excess AR solution was removed after staining and samples washed 3 times with distilled water. For quantitative analysis, 5% v/v perchloric acid in distilled water was used to destain AR on a platform rocker at 30 rpm for 24 h. The absorbance of the eluate was read with the spectrophotometer at 405 nm.

2.12. Histology

Histological samples were taken as complete transverse-sections across the centre of electrospun scaffolds. Samples were fixed with 3.7% formaldehyde, soaked in 1% sucrose solution and embedded in OCT^{TM} compound media prior to sectioning. Samples were cryo-sectioned at 15 μm and stained with Haematoxylin and Eosin. Stained sections were imaged with a light microscope with 20 × objective.

2.13. Statistical analysis

All data are reported as mean±standard deviation. Comparison of sample means of fibre diameter and mechanical analysis was performed by one-way analysis of variance using GraphPad Prism 6 software, whilst MTT cell viability, calcium and collagen absorbance data were analysed by two-ways repeated measures analysis of variance. Differences between two groups were defined as statistically significant if $p \leq 0.05$ as determined by the Tukey's multiple comparisons post hoc test.

3. Results and discussion

Bone, the major load bearing tissue of the human body is subjected to varying degrees of loading and unloading on a daily basis. Hence, designing a scaffold for bone tissue engineering requires a material that is mechanically compatible, that should be able to undergo varying degrees of deformation without rupturing. Polyurethane remains a popular choice amongst polymers for its advantageous properties of biocompatibility, biodegradability, mechanical flexibility and versatile chemistry allowing it to be tailor-made for specific applications.

3.1. PU scaffolds

Microphase segregation, a key characteristic of thermoplastic polyurethane elastomers occurs as a result of the thermodynamic incompatibility of the hard and soft segments of PU and is known to play a key role in the mechanical properties of PU. Factors known to affect the degree of separation include segment polarity, hydrogen bonding responsible for hard/soft segment interaction, overall sample constitution and molecular weight. Thermoplastic elastomers with different molecular weights Z9A1 and Z3A1 but identical chemical structures and composed of 4,4′-diphenylmethane diisocyanate, polyether diol, and 1,4 butane diol were dissolved in graded concentrations of DMF and THF to study the effect of solvent combination on electrospun fibre morphology and mechanical properties. DMF and THF are popular solvents used in dissolving and synthesising polyurethane (Khil et al., 2003; Tsui and Gogolewski, 2009). These solvents differ in polarity, evaporation rate, and conductivities, which are key parameters that affect electrospinning and microphase segregation.

Scaffolds fabricated from solution containing 100% DMF had more nano-diameter fibres and beads than other solvent combinations of DMF and THF for both types of PU (Fig. 1). Reducing the amount of DMF, by replacing with THF eliminated the presence of beads and resulted in fibres with a more uniform morphology for Z9A1 scaffolds, and a combination of nano and micro fibres for Z3A1 scaffolds. For both types of PU, scaffolds made from solutions containing 50% THF solvent had fibres with significantly larger diameters to those fabricated from 100% DMF and 70/30 DMF/THF combinations. We cannot directly compare the effects of molecular weight (Z3A1 versus Z9A1) in this study as spinning parameters were also slightly different between these two sets of scaffolds. However in general, Z3A1 dissolved faster and more uniformly than Z9A1 prior to electrospinning, presented with a more uniform viscosity and was easier to fabricate. Armentano et al. (2010) reported that the solvent choice used in fabricating polymer films influences several scaffold properties, including the heterogeneity of the surface structure, reorientation or mobility of the surface crystal segment, as well as swelling and deformation. In our study, differences in electrospun morphology which resulted from changing the amount of DMF contained in solution is supported by the work of Oprea, (2005) who studied the effect of N-methyl-2-pyrrolidone (NMP), DMF, toluene and ethyl acetate on the properties of polymer films, and reported differences in morphology and mechanical properties of films fabricated from solutions containing NMP and DMF solvents. They suggested that NMP was a better solvent than DMF for developing polyurethane films. Wannatong et al., (2004) also studied the effect of five different solvents on electrsospun polystyrene (PS) and reported that DMF was the best solvent for preparing beadless PS scaffolds. This is in contrast to what was observed in our study, but these different results could be due
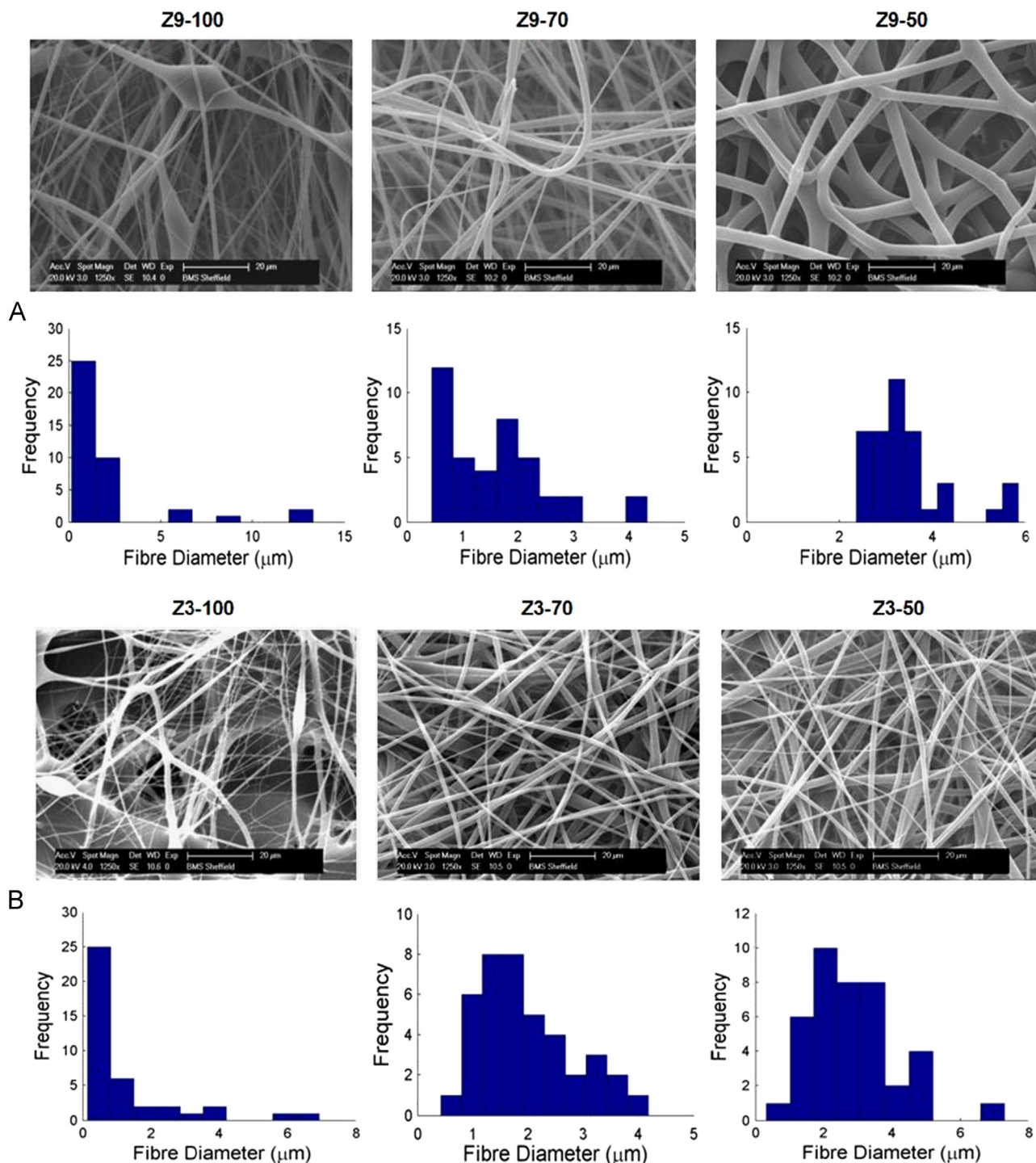
Fig. 1 – SEM images of electrospun (A) Z9A1 and (B) Z3A1 scaffolds synthesised with different combinations of DMF & THF (scale bar=20 μm), and (below) a histogram of the fibre diamter (n=40).

to differences in concentration of solutions, molecular weights and polymer choice, as PU and PS have different chemical and physical properties.

3.2.   PU–HA composites

Mimicking the ductile properties of collagen and the strength of the mineralised phase of bone with PU and HA particles combined in micro or nano composites has been proposed for bone substitute materials for a number of reasons. The elastomeric nature of PU serves as a matrix, reinforced by the HA particles. Nano HA and micro HA differ in several ways including surface area and the degree of crystallinity which both affect overall sample constitution. By including both particle types in separate solutions, we were able to assess the effect

of particle size on fibre morphology and mechanical properties.

Note that the PU scaffolds without HA for this set of experiments were spun from a 70/30 solution of DMF/THF because this enabled the best fibre morphology (without beads), however the processing conditions for Z9-PU and Z3-PU are slightly different from those used in the Z9-70 and Z3-70 groups (Table 1) so these are not expected to have identical morphological and mechanical properties.

Electrospun 25 wt% Z9A1 and 15 wt% Z3A1 dissolved in 70/30 DMF/THF solvents showed relatively uniform fibre diameter distributions. However, the inclusion of mHA and nHA particles resulted in changes to fibre morphology. For both types of PU, nHA particles with a higher surface area and smaller particle size, blended well with PU and resulted in more uniform fibres compared to composite scaffolds containing mHA particles, which presented with a beaded morphology and generally reduced fibre diameters (Fig. 2) but with some particularly large
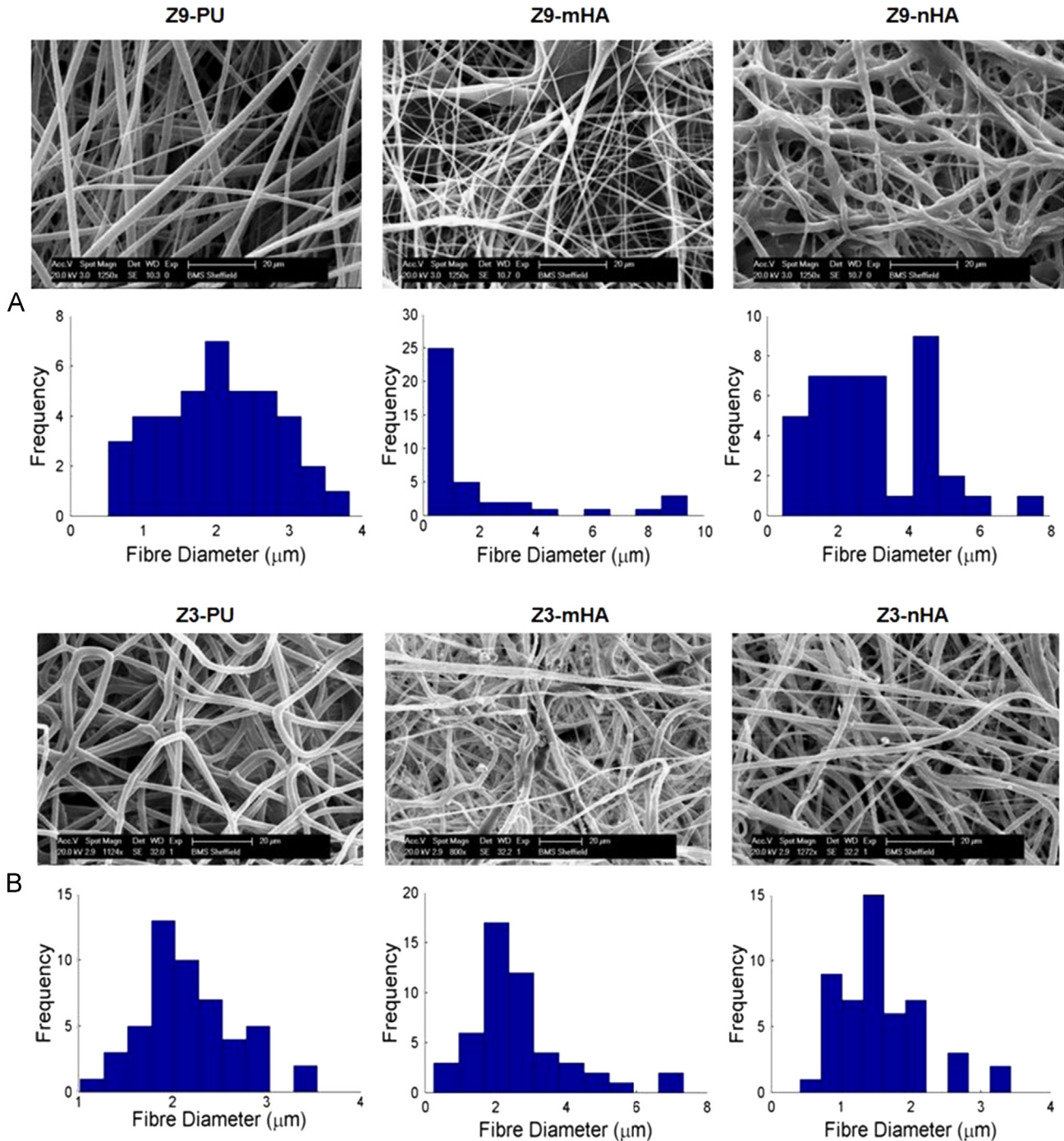
Fig. 2 – SEM images of electrospun (A) Z9A1 and (B) Z3A1 PU (left column), mHA (middle column) and nHA (right column) composite scaffolds (scale bar=20 μm), and (below) a histogram of the fibre diamter (n=40). Note that the axes for each histogram are to different scales reflecting the varibility in fibre size between scaffold compositions and the histogram for Z9-mHA excludes a single 35 μm fibre which is included in the mean values presented in Table 3.

fibres. It is likely that the particularly large fibres contain large chunks of mHA leading to a bimodal distribution of fibre size and large standard deviation (Table 2). There was a single extremely large fibre of 35 μm in the field of view examined which was not included in the frequency plot (Fig. 2A) as it would have made it difficult to visualise the rest of the data but this is included in the fibre average diameter data (Table 2).

Reduction in fibre diameter with the inclusion of mHA particles to create composites was also observed by Nirmala et al. (2011) who electrospun nanofibrous polyurethane with micro Calcium Chloride particles and by Mi et al. (2014) who suggested that that mHA particles may have stretched the polymer jets while the fibres were being deposited. The effect of more fibres at a lower diameter and a few fibres at a much larger diameter caused by the inclusion of mHA is much less marked when the Z3A1 polymer is used, this may be explained by smaller molecular weight and polymer chain length of Z3A1 compared to Z9A1 and lower viscosity.

It has been reported that the higher surface area of nHA compared to mHA enables better bonding between the nano-sized HA particles and PU enabling greater reinforcement of the polymer matrix and ultimately, enhancing mechanical and functional properties of nanocomposites compared to conventional microcomposites (Armentano et al., 2010). This probably explains why the nHA fibres are much more consistent in their size and morphology as the particles would be better distributed within, and bound to, their polymer matrix.

3.3. FTIR characterisation

The polar nature of PU and HA makes FTIR characterisation, which elicits differences in dipole moments, an ideal characterisation technique for analysing the chemical composition of composite scaffolds. The FTIR spectrum of polyurethane is presented in Fig. 3A, and the combined spectra of PU–HA composites are presented in Fig. 3B and C

For PU, the peak at $3325\ cm^{-1}$ is attributed to the stretching υ(N–H). The peak at $3121\ cm^{-1}$ was the overtone of $1533\ cm^{-1}$ and $3039\ cm^{-1}$ attributed to the υ(C–H) in benzene ring. The peaks at 2940, 2857 and $2795\ cm^{-1}$ were CH_2 peaks of the polyether. The peak at $2940\ cm^{-1}$ was the asymmetric stretching peak of CH_2 and the peak at $2857\ cm^{-1}$ was the symmetric stretching of CH_2. The carbonyl absorption region was observed in between 1730 and $1700\ cm^{-1}$, the carbonyl absorption band classified into two peaks. The peak due to bonded C=O stretching was at $1701\ cm^{-1}$ and the free C=O stretching appeared at $1730\ cm^{-1}$. The peak at $1597\ cm^{-1}$ was assigned to υ(C=C) in the benzene ring and $1533\ cm^{-1}$ was the amide II δ (N–H)+υ(C=N). $1478\ cm^{-1}$ was the weak CH_2 peak and the $1413\ cm^{-1}$ attributed to the strong υ(C–C) in benzene ring. The peak at $1310\ cm^{-1}$ was assigned to amide III δ(N–H)+υ(C=N), β(C–H) peak and δ(N–H)+υ(C=N) appeared at $1225\ cm^{-1}$. The region between 1103 and $916\ cm^{-1}$ was the υ(CH_2–O–CH_2) of ether peak and $1018\ cm^{-1}$ was the weak β(C–H) in benzene ring. The peak at $817\ cm^{-1}$ was the γ(C–H) from butane diol. These observations were similar to those reported by Khan et al. (2008) in their study of polyurethane composites for dental restoration applications.

Fig. 3B shows the combined spectra of Z3-PU, Z3-mHA and Z3-nHA at common scale, with emphasis on the hydroxyl, carbonyl, phosphate and bending phosphate groups whilst Fig. 3C shows the combined spectra in greater detail for a wave number region of $1800-450\ cm^{-1}$. The characteristic peak of stretching O–H was observed at $3570\ cm^{-1}$ (Rehman and Bonfield, 1997). The bands at 1060, 961, 603 and $571\ cm^{-1}$ were assigned to vibration of the phosphate group, PO_4. The peak at $1078\ cm^{-1}$ was the triply degenerated vibration v_3, and $961\ cm^{-1}$ was the non-degenerated symmetric stretching mode v_1, of the P–O bond of the phosphate group. The peaks at 603 and $571\ cm^{-1}$ were assigned to a triple degenerated bending mode v_4, of the O–P–O bond. The peak at $633\ cm^{-1}$ was due to the phosphate v_4 bending. The stretching O–H and P–O (stretching and bending) peaks were not present in the polyurethane spectrum. After mixing the micro and nano hydroxyapatite in polyurethane, the appearance of characteristic peaks of HA were observed and it was noted from the shifting and appearance of new peaks in the region of 1100–$916\ cm^{-1}$ that nano-HA with a higher surface area and more crystalline structure was mixed better than micro-HA and affected the shifting of peaks v_3 P–O from $1078\ cm^{-1}$ for Z3-mHA to $1060\ cm^{-1}$ for Z3-nHA. It has been mentioned in the literature that the width and intensity of peaks in FTIR spectrum have explicit dependence on the particle size. As particle size increases, the width of the peak decreases and intensity increases. The restoring force of nano particles created by surface polarisation charge is responsible for the frequency difference. The difference in the frequency of vibrational modes is attributed to dipolar interactions,

Table 2 – Morphological and mechanical properties of Z9A1 and Z3A1 scaffolds with different solvent combinations (mean±S.D., $n=40$ for fibre measurements and 6 for all other measurements).

Electrospun Scaffolds	Fibre diameter (μm)	Thickness (mm)	Young's modulus (MPa)	Yield strength (MPa)
Z9-100	2.06 ± 3.09^{c}	0.27 ± 0.02	$60.09\pm10.1^{b,c}$	2.13 ± 0.55^{c}
Z9-70	1.54 ± 0.96^{c}	0.29 ± 0.06	25.89 ± 4.54^{a}	1.73 ± 0.79
Z9-50	$3.47\pm0.89^{a,b}$	0.36 ± 0.04	30.11 ± 0.78^{a}	1.27 ± 0.29^{a}
Z3-100	$1.25\pm1.56^{b,c}$	0.06 ± 0.01	$18.54\pm2.31^{b,c}$	$1.56\pm0.34^{b,c}$
Z3-70	$1.93\pm0.85^{a,c}$	0.18 ± 0.03	7.61 ± 0.76^{ac}	0.71 ± 0.03^{a}
Z3-50	$2.82\pm1.29^{a,b}$	0.10 ± 0.01	$3.38\pm1.25^{a,b}$	0.50 ± 0.04^{a}

[a] Significantly different from scaffolds made from 100% DMF, at $p \leq 0.05$.
[b] Significantly different from scaffolds made from 70/30 DMF/THF, at $p \leq 0.05$.
[c] Significantly different from scaffolds made from 50/50 DMF/THF, at $p \leq 0.05$.

Table 3 – Morphological and mechanical properties of Z9A1 and Z3A1 scaffolds with different types of HA, (mean±S.D., $n=40$ for fibre measurements and 6 for all other measurements).

Electrospun Scaffolds	Fibre diameter (µm)	Thickness (mm)	Young's modulus (MPa)	Yield strength (MPa)
Z9-PU	2.01±0.80	0.36±0.01	9.56± 3.03[b]	0.61±0.18[b]
Z9-mHA	2.86±6.01	0.30±0.01	88.69±20.20[a,c]	3.02±0.80[a,c]
Z9-nHA	2.95±1.60	0.42±0.02	10.21±2.99[b]	0.79±0.16[b]
Z3-PU	2.18±0.51[c]	0.43±0.09	2.42±0.21[b,c]	0.29±0.04[b,c]
Z3-mHA	2.61±1.45[c]	0.31±0.01	4.77±0.29[a,c]	0.46±0.03[a]
Z3-nHA	1.56±0.63[a,b]	0.09±0.01	3.09±0.30[a,b]	0.52±0.09[c]

[a] Significantly different from PU scaffolds, at $p \leq 0.05$.
[b] Significantly different from scaffolds made with mHA, at $p \leq 0.05$.
[c] Significantly different from scaffolds made with nHA, at $p \leq 0.05$.
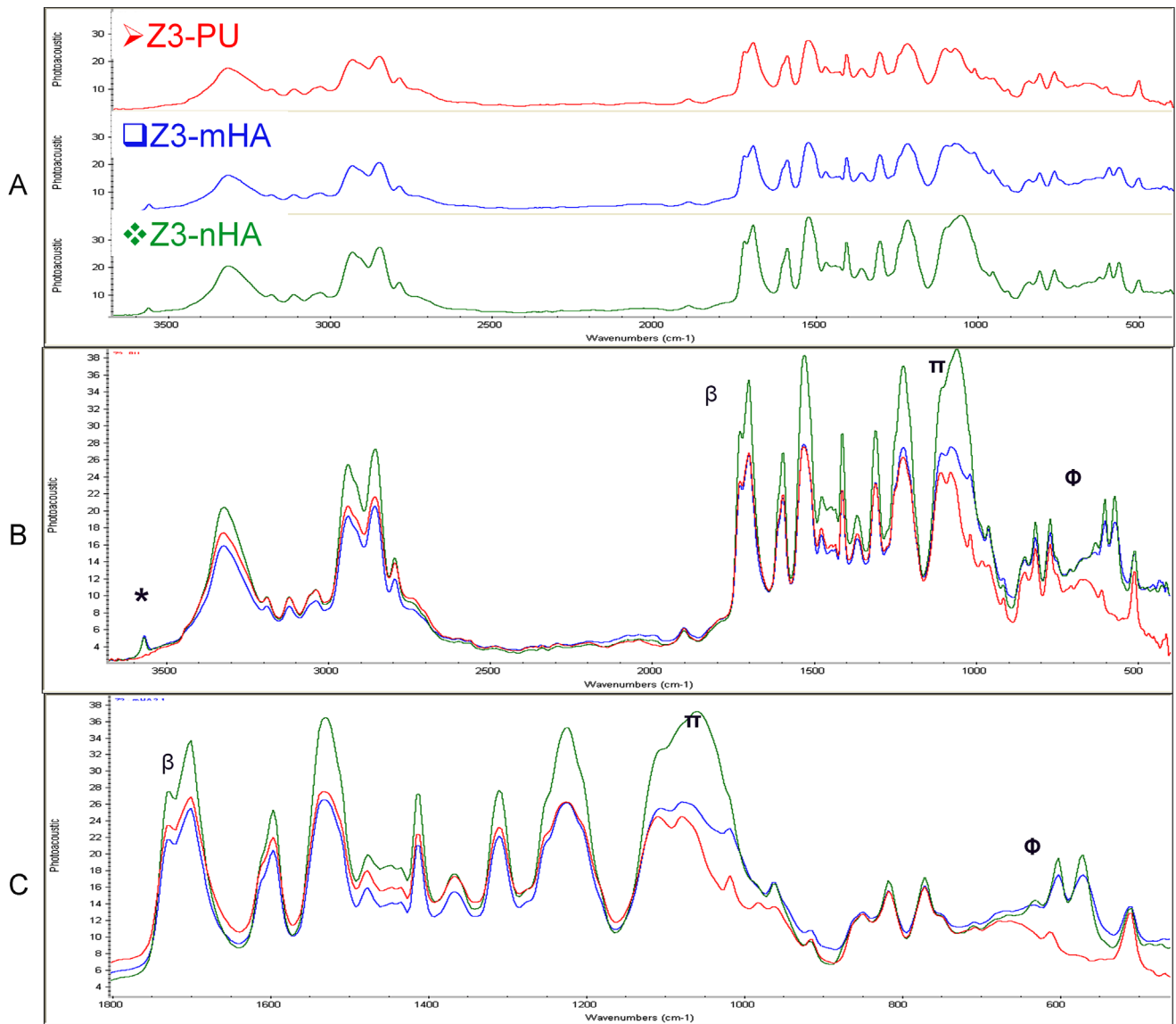
Fig. 3 – FTIR spectra of Z3A1 composites (A) stacked FTIR spectra of Electrospun Z3-PU, Z3-mHA and Z3-nHA. (B) Combined FTIR spectra of Z3-PU, Z3-mHA and Z3-nHA at Common Scale with Hydroxyl, Carbonyl, Phosphate and bending Phosphate groups highlighted as *, β, π and Φ, respectively. (C) Combined spectra of Z3-PU, Z3-mHA and Z3-nHA at common scale for a wavenumber region of $1800-450\ cm^{-1}$.

interfacial effects, surface amorphousness, surface free energy etc. (Mo et al., 1993; Martin, 1996; Bobovich, 1988).

3.4. Mechanical analysis of PU scaffolds

In general, Z9A1 scaffolds were stronger than Z3A1 scaffolds and presented with higher mechanical properties for all combinations of DMF and THF solvents. With identical chemical structures, differences in the mechanical properties of Z9A1 and Z3A1 probably resulted from the differences in molecular weights, which would have affected the interaction between the hard and soft segments, causing differences in the microphase segregation.

Decreasing the proportion of DMF in the solvent reduced Young's Modulus and strength of Z9A1 and Z3A1 scaffolds. Z9-100 (100% DMF) showed a brittle stress-strain profile with plastic deformation occurring at 30% strain (Fig. 4A). Z9-100 also had the highest Young's Modulus and yield strength, significantly higher than those of Z9-50 for both properties, however, only Young's Modulus was significantly higher than that of Z9-70 scaffolds (Table 2).

A similar pattern was observed with the Z3 groups (Fig. 4B). Values of Young's Modulus for Z3-100, Z3-70 and Z3-50 were significantly reduced with less DMF in the electrospinning solvent (Table 1). For both polymers these differences in mechanical properties are likely to be the result of differences in fibre morphology (Fig. 1) which in turn may have resulted from differences in the solvent properties of DMF and THF. Beads present in scaffolds fabricated with 100% DMF solvent (Fig. 1) probably created short regions of

large fibre cross-sectional area, which would have caused there to be a greater amount of material relative to void space within the sample, which would in turn create an overall stronger scaffold but with a reduced ability to undergo strain.

3.5. Mechanical analysis of PU–HA composites

Mechanical properties of composites are controlled by several micro-structural factors such as the properties of the matrix, the properties and distribution of fillers, interfacial bonding strength, and processing methods. The interface strength between PU and HA particles greatly affects the effectiveness of load transfer from the polymer matrix to micro and nanocomposites. For composite scaffolds, inclusion of HA particles improved the tensile properties of both Z9A1 and Z3A1 scaffolds, Young's Modulus and yield strength of composite scaffolds were significantly higher than those of plain PU scaffolds, for both Z9A1 and Z3A1. SEM images of electrospun composites (Fig. 2) show that nHA, with its smaller size and higher surface area, properly integrated with the PU fibres compared to mHA which can be seen sticking out of the fibres and creating lumps and beads. Better mixing of nHA particles with PU as compared to mHA particles was also confirmed with FTIR for Z3-composites. We therefore expected that the nano-composites would be stiffer and stronger than the micro-composites However, for Z9A1, both yield strength and Young's Modulus of mHA scaffolds were significantly higher than those of Z9-nHA scaffolds. Interestingly, the yield strength of Z3-nHA scaffolds was higher than that of Z3-mHA, although not statistically
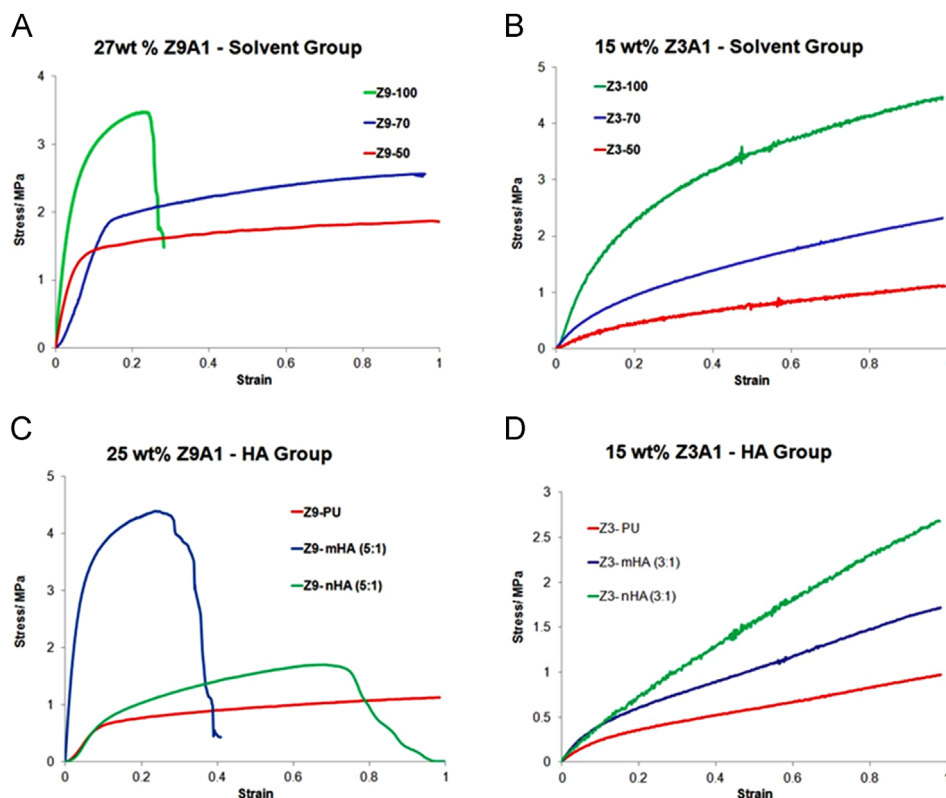
Fig. 4 – Example stress/strain curves of fabricated scaffolds, (A) effect of solvent combination on Z9A1 scaffolds, (B) effect of solvent combination on Z3A1 scaffolds, (C) effect of HA particles on Z9A1 scaffolds, (D) effect of HA particles on Z3A1 scaffolds.

significant. These differences in behaviour between Z9A1 and Z3A1 composite scaffolds could have resulted from the difference in the PU:HA ratio between Z9A1 (5:1) and Z3A1 (3:1) and the molecular weight of the polymers. Z9A1 is of higher molecular weight and produces scaffolds that are high in Young's modulus and strength but more brittle, the addition of HA further increases the brittleness of the electrospun scaffold. In contrast, Z3 is of lower molecular weight and more flexible and the addition of HA, albeit at a higher concentration that for Z9, has a smaller effect on the properties of the electrospun scaffold. Molecular weight and concentration and size of HA would all have resulted in differences in interactions between solvents, macromolecular chains of the polymer and the HA particles. These difference in interactions have been reported to affect microphase separation between the hard and soft segment of PU, hence ultimately affecting its mechanical properties (Oprea, 2005).

3.6.   Cell viability on PU Scaffolds

The MLO-A5 mouse cell line has characteristics of a post-osteoblast and pre-osteocyte cell type, and rapidly mineralises in sheets rather than nodules. These cells have been used to extensively study the osteoblast to osteocyte differentiation process, bone mineralisation and the effects of mechanical loading on biomineralization (Sittichockechaiwut et al., 2009,

Rosser and Bonewald, 2012). MLO-A5 cells were seeded on Z9A1 and Z3A1 PU scaffolds fabricated from solutions containing varying combinations of DMF/THF solvents.

In general, cells were viable on all scaffolds during the 14 day culture period. Cells had similar viability on all Z9A1 on day 1, indicating that, there were no differences in the cell's ability to attach to scaffolds. Viability increased steadily from day 1 to day 4 with similar values on Z9-100 and Z9-70 scaffolds between day 4 and day 7. On day 14 of culture, there was no significant difference between MTT absorbance on Z9-70 and Z9-100, however, cell viability on Z9-50 scaffolds was significantly lower than that of Z9-100 and Z9-70 ($p \leq 0.05$) (Fig. 5A). This could have been the result of morphological differences in fibre diameter, as Z9-50 fibre diameters were significantly larger than Z9-70 and Z9-100 scaffolds.

For Z3A1 scaffolds, there was a steady increase in cell viability on all Z3-100, Z3-70 and Z3-50 scaffolds during the culture period (Fig. 5B). There was however, no significant difference between all groups of scaffolds, except that Z3-50 supported lower cell viability on day 4 ($p \leq 0.05$). The ability of electrospun scaffolds to mimic the natural three-dimensional environment of the *in vivo* extracellular matrix whilst providing structural support with high surface to volume ratio makes excellent structures for tissue engineering applications. It has been reported that cells assume a more spindle-shaped morphology with increasing fibre diameters and rather orient parallel to fibres with aligned meshes (Bashur et al., 2009,
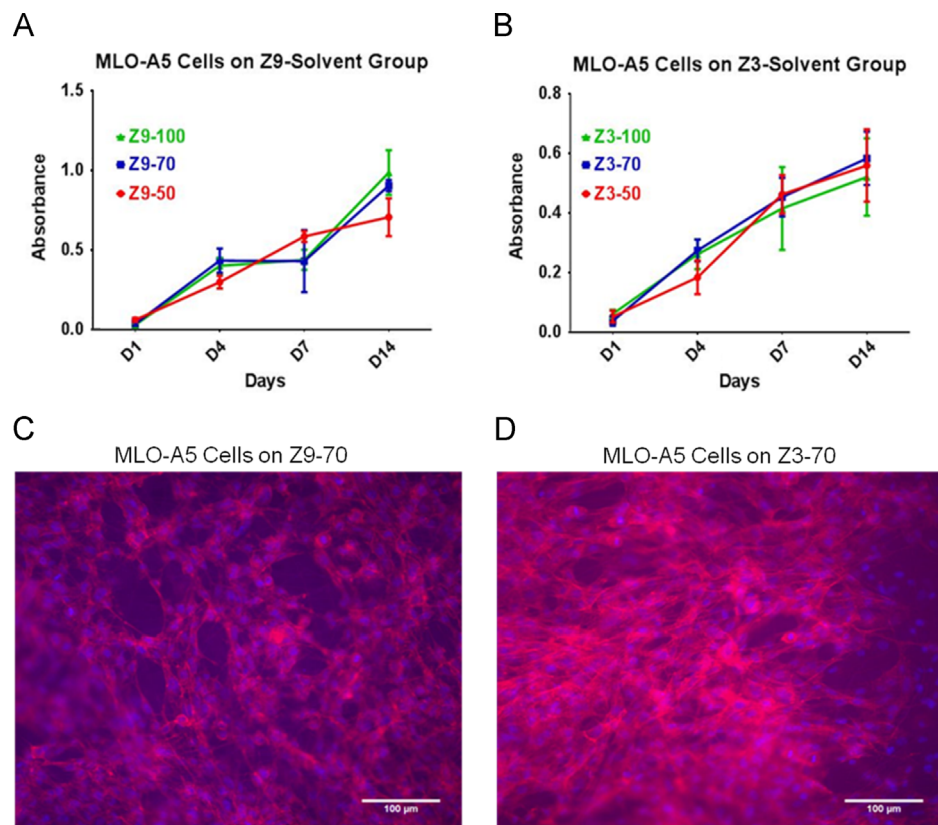
Fig. 5 – MTT absorbance for MLO-A5 cells seeded on (A) Z9A1 PU scaffolds, (B) Z3A1 PU scaffolds (mean±S.D. $n=6$) for statistical analysis see text. (C) and (D) Fluorescent micrographs of DAPI (blue=nucleus) and phalloidin (red=actin) staining of MLO-A5 Cells on Z9-70 (C) and Z3-70 (D) scaffolds on day 4, scale bar at 100 μm. (For interpretation of the references to colour in this figure legend, the reader is referred to the web version of this article.)

Delaine-Smith et al., 2014). DAPI (nucleus) and Phalloidin (actin cytoskeleton) staining over a seven day period confirmed the MTT data indicating increasing numbers of cells attached to the scaffolds over time (data not shown). Fig. 5 shows representative micrographs of cell attachment on day 4 indicating that cells are well spread across the scaffolds with an elongated morphology for Z9-70 (Fig. 5C) and Z3-70 (Fig. 5D) scaffolds.

3.7. Cell viability on composite scaffolds

Hydroxyapatite ($Ca_{10}(PO_4)_6(OH)_2$), HA is well established as a synthetic material for bone replacement due to its chemical resemblance to the inorganic component of bone and tooth, and has been widely used a biocompatible material in many areas of medicine. HA is known to promote faster bone regeneration and direct bonding to regenerated bone without intermediate connective tissue (Patel et al., 2002).

For composite scaffolds, Z3A1 scaffolds consistently presented with a more uniform combination of nano and micro fibre diameters and were less brittle than Z9A1 composites, therefore Z3A1 was used to examine the effect on cell behaviour of including HA in the scaffold. MLO-A5 cells seeded on Z3-nHA scaffolds had the highest cell viability at all-time points after day 1, being 22% higher by day 28 (Fig. 6A), this implies that cell proliferation rate was higher on these scaffolds as MTT absorbance at day 1 was the same for all groups. This is similar to the effects of nHA observed in previous studies (Rezwan et al., 2006; Bianco et al., 2009; Mi et al., 2014) and probably resulted from the bioactive nature of HA coupled with the higher surface area and crystallinity of nHA particles. A high HA surface area facilitates a strong interaction between the polymer and ceramic phase, and allows protein attachment. For example, it has been reported that initial calcium absorption to nanoceramic surfaces enhanced binding of vitronectin, that subsequently promoted osteoblastic adhesion and proliferation (Webster et al., 2001). It might be expected that mHA would also elicit cell viabilities as high as those attained by the nano-composites but that was not observed for MLO-A5 in this study. This may have been due to the lower porosity that was observed with the inclusion of mHA particles, which could have hindered cell proliferation, migration, and nutrient transfer.

To investigate the ability of these composites to support progenitor cells, hES-MPs, embryonic derived mesenchymal progenitor cells were also seeded on Z3A1 electrospun scaffolds in osteogenic media (Fig. 6B). hES-MPs have been used in several studies as a model cell for bone tissue engineering (Karlsson et al., 2009). In the presence of osteogenic supplements, hES-MP cells have been shown to differentiate towards the osteogenic lineage in vitro (Delaine-Smith et al., 2012). Such mesenchymal progenitor cells also may have advantages over autologous bone marrow derived mesenchymal stem cells for clinical tissue engineering as they are readily available in large numbers and would avoid the extraction and expansion steps needed to tissue engineer bone from a patient's own cells.

As shown in Fig. 6B, there was an increase in hES-MP cell viability over all time-points on Z3A1 scaffolds however, in contrast to MLO-A5 cells; there was no significant difference between Z3-nHA, Z3-mHA and Z3-PU scaffolds in their ability to support cell proliferation. There is no obvious reason for this different effect of nHA on cell proliferation of the two types it but may be related to their different stages in the osteogenic differentiation pathways.

3.8. Collagen and calcium staining and histology

The ultimate test of a scaffold's ability to support bone tissue engineering is its ability to support bone-like extracellular matrix deposition. Collagen and calcified matrix staining using Sirius red and alizarin red, respectively were used to study extracellular matrix production and mineralisation on days 14, 21 and 28 of culture. Collagen production by MLO-A5 cells on Z3 scaffolds was highest for Z3-nHA scaffolds at all-time points (Fig. 7A) with the highest deposition measured on day 28, significantly higher than that produced on Z3-mHA and Z3-PU scaffolds. This is the same scaffold that supported the highest number of viable MLO-A5 cells. A similar pattern was observed with hES-MP cells (Fig. 7B).

Interestingly, calcium production elicited results opposite to those attained for collagen production. Alizarin red absorbance on of cell-seeded Z3–PU scaffolds was higher for both MLO-A5 (Fig. 7C) and hES-MP cells (Fig. 7d) than for HA composite scaffolds (after substraction of the background absorbance). However, unsurprisingly, alizarin red strongly stained the blank
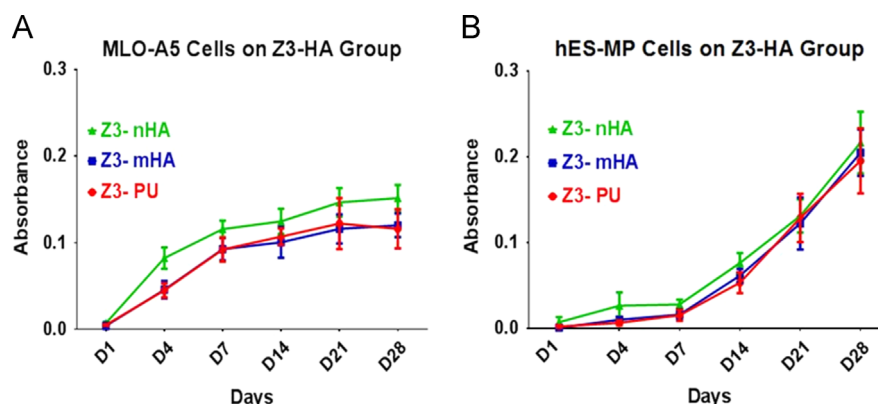
Fig. 6 – MTT absorbance on Z3A1 composite scaffolds (mean ± S.D. $n = 6$). (A) MLO-A5 cells on Z3 PU, Z3-mHA and Z3-nHA scaffolds, (B) hES-MP cells on Z3 PU, Z3-mHA and Z3-nHA scaffolds. For statistical analysis see text.
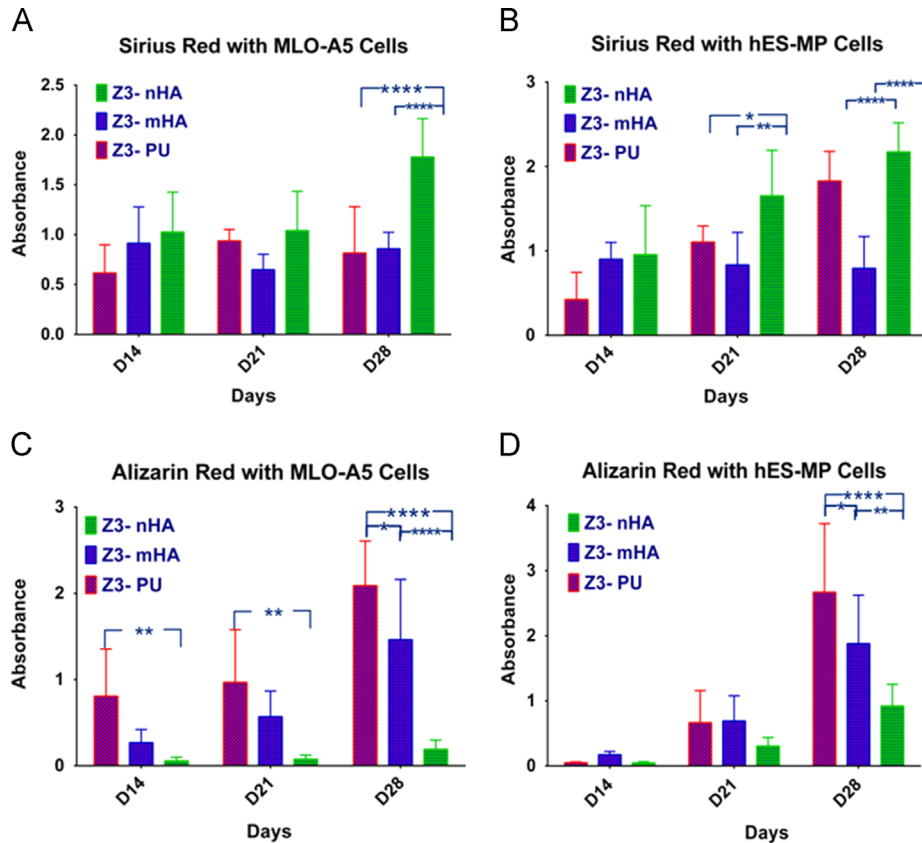
Fig. 7 – Collagen and calcium Staining on Z3-PU, Z3-mHA and Z3-nHA scaffolds on D14, D21 and D28 (mean ± S.D. $n=6$). (A) sirius red absorbance of MLO-A5 cells, (B) sirius red absorbance of hES-MP cells, (C) alizarin red absorbance of MLO-A5 cells (D) alizarin red absorbance of hES-MP cells. $*p \leq 0.05$, $** \leq 0.01$, $**** \leq 0.0001$. (For interpretation of the references to colour in this figure legend, the reader is referred to the web version of this article.)

(no cells) control scaffolds that contained HA. As this is a single blank and not the same sample on which cells are seeded, any variability in HA content between scaffold samples would have made it more difficult to distinguish between the scaffold HA and cell-deposited HA. It would be interesting to image mineralisation in the same scaffold over time using a technique such as µCT scanning or Xylenol orange to determine if there was truly less cell deposited calcium in composite scaffolds.

Histological sections were taken to examine how far MLO-A5 and hES-MP cells penetrated into the Z3 PU and composite scaffolds by day 14 of culture, having been seeded at the surface (Fig. 8). In general, MLO-A5 cells were densely distributed on the surface of all scaffolds as compared to hES-MP cells which exhibited thinner coverage in Z3-PU and Z3-mHA scaffolds and were more loosely dispersed throughout the scaffold interior. hES-MPs cells cultured on Z3-nHA scaffolds appeared to penetrate to the greatest depth and were found in more locations compared to all other groups, although no cells were seen at the bottom of the scaffold at this time-point. The lack of cell penetration into the scaffold may have resulted from the low porosity, pore size and interconnectivity of scaffolds associated with the closely packed arrangement of the fibres. It is interesting that hES-MPs appear to penetrate deeper than MLO-A5s, which may be related cell size or differences in attachment and migration cell surface molecules. This observation has also been reported extensively in the literature as a major limitation of

traditional electrospun sheets (Bergmeister et al., 2013; Leong et al., 2010). It would therefore be advantageous to increase the porosity of electrospun scaffolds by opening up spaces between the fibres. Electrospinning with a cryogenic mandrel, controlling fibre deposition with air-flow impedance and electrospinning with porogens, amongst others, have reported to enhance scaffold porosity and cell penetration (McClure et al., 2012). It is also possible to increase porosity by co-spinning polymer solutions with a very fast degrading or water-soluble polymer (Milleret et al., 2011), and using mechanical techniques such as ultrasonication (Lee et al., 2011) and static stretch to force fibres apart and thus facilitate greater cell penetration, nutrient diffusion and transport of metabolic products.

4. Conclusions

Choice of solvents, on their own or in combination, strongly influences the final properties of solution, hence fibre morphology during the electrospinning process. Two types of thermoplastic polyurethane Z9A1 and Z3A1 were electrospun from solutions made with varying combinations of DMF and THF solvents. For both types of PU reducing the amount of DMF contained in the solution, increased fibre diameter, resulting in fibres with a more uniform morphology, and also eliminating the beads which were found in the scaffolds fabricated from 100% DMF solvent.
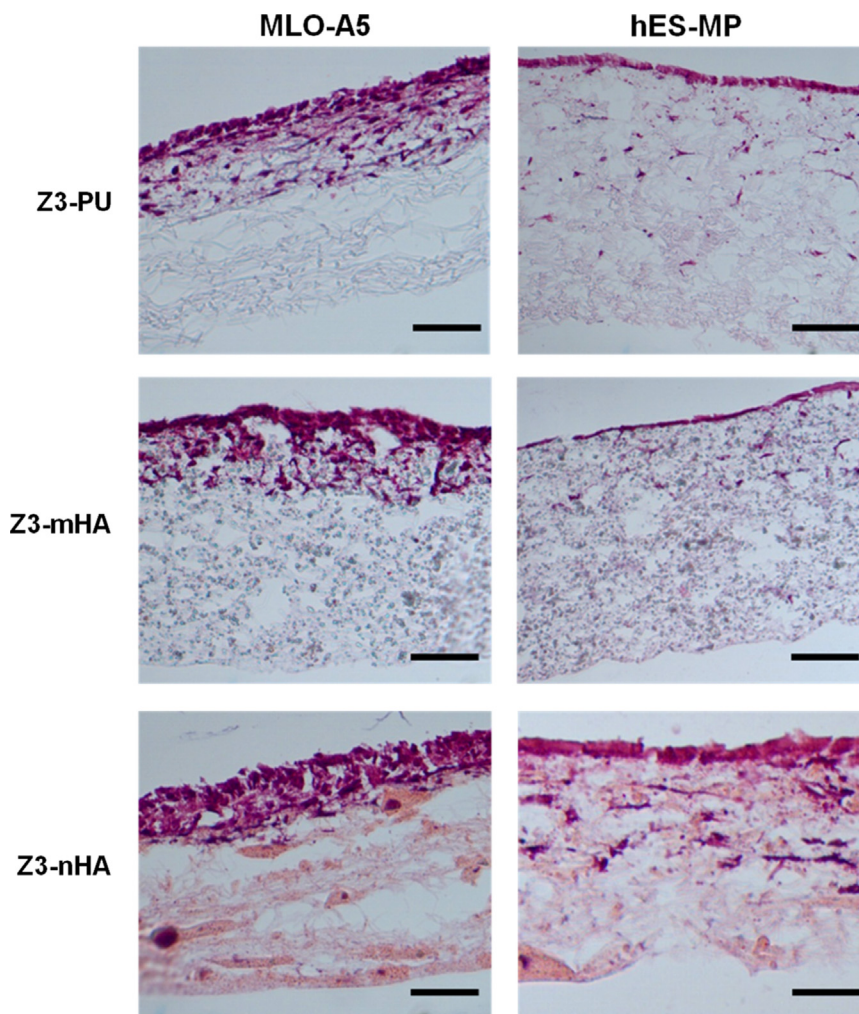
Fig. 8 – H&E staining on Z3-PU, Z3-mHA and Z3-nHA scaffolds on Day 14 of culture for MLO-A5 and hES-MP cells. Scale Bar at 100 μm.

In addition, reducing the DMF solvent content led to lower tensile properties of electrospun scaffolds, whilst incorporation of nano and micro HA particles in both Z9-PU and Z3-PU solutions reinforced the mechanical properties of electrospun composites. Young's Modulus and yield strength values of composites were higher than that of PU scaffolds; these differences were significantly higher with mHA composites compared to nHA composites but nHA composites exhibited smoother fibres, less variability in fibre size and better dispersion of the HA. Furthermore, FTIR spectral data confirmed the presence of HA particulates in fabricated composites.

Finally, MLO-A5 cell viability was highest for scaffolds fabricated with 70/30 DMF/THF solvent across most time points for both types of PU, whilst cell viabilities for both MLO-A5 and hES-MP cells, were highest with Z3-nHA scaffolds which also produced the highest deposition of collagen across all time points. Calcium deposition was supported in all scaffolds. Therefore, we have developed a range of scaffolds which have the potential to support bone matrix formation for bone tissue engineering, providing varying material properties which can be tailored depending on the stage of cell differentiation and final application.

Acknowledgements

REFERENCES

Adhikari, R., Gunatillake, P.A., Griffiths, I., Tatai, L., Wickramaratna, M., Houshyar, S., Moore, T., Mayadunne, R.T. M., Field, J., Mcgee, M., Carbone, T., 2008. Biodegradable injectable polyurethanes: synthesis and evaluation for orthopaedic applications. Biomaterials 29, 3762–3770.

Armentano, I., Dottori, M., Fortunati, E., Mattioli, S., Kenny, J.M., 2010. Biodegradable polymer matrix nanocomposites for tissue engineering: a review. Polym. Degrad. Stabil. 95, 2126–2146.

Attawia, M., Herbert, K., Laurencin, C., 1995. Osteoblast-like cell adherance and migration through three-dimensional porous polymer matrices. Biochem. Biophys. Res. Commun. 213, 639–644.

Bashur, C.A., Shaffer, R.D., Dahlgren, L.A., Guelcher, S.A., Goldstein, A.S., 2009. Effect of fiber diameter and alignment of electrospun polyurethane meshes on mesenchymal progenitor cells. Tissue Eng. Part A 15, 2435–2445.

Bergmeister, H., Schreiber, C., Grasl, C., Walter, I., Plasenzotti, R., Stoiber, M., Bernhard, D., Schima, H., 2013. Healing characteristics of electrospun polyurethane grafts with various porosities. Acta Biomater. 9, 6032–6040.

Bianco, A., Federico, D.I., Moscatelli, E., Camaioni, I., Armentano, A., Campagnolo, I., Dottori, L., Kenny, M., Siracusa, G., J.M., Gusmano, G., 2009. Electrospun poly(ε-caprolactone)/Ca-deficient hydroxyapatite nanohybrids: Microstructure, mechanical properties and cell response by murine embryonic stem cells. Mater. Sci. Eng.: C 29, 2063–2071.

Bobovich, Y.S., 1988. Classical size effects in the Raman scattering spectra of highly dispersed particles. Experimental studies (review). J. Appl. Spectrosc. 49, 869–888.

Boccaccini, A.R., Maquet, V., 2003. Bioresorbable and bioactive polymer/Bioglass® composites with tailored pore structure for tissue engineering applications. Compos. Sci. Technol. 63, 2417–2429.

Boissard, C., Bourban, P.-E., Tami, A., Alini, M., Eglin, D., 2009. Nanohydroxyapatite/poly (ester urethane) scaffold for bone tissue engineering. Acta zBiomater. 5, 3316–3327.

Bonfield, W., 1988a. Composites for bone replacement. J. Biomed. Eng. 10, 522–526.

Bonfield, W., 1988b. Hydroxyapatite-reinforced polyethylene as an analogous material for bone replacementa. Ann. NY Acad. Sci. 523, 173–177.

Bonzani, I.C., Adhikari, R., Houshyar, S., Mayadunne, R., Gunatillake, P., Stevens, M.M., 2007. Synthesis of two-component injectable polyurethanes for bone tissue engineering. Biomaterials 28, 423–433.

Bose, S., Roy, M., Bandyopadhyay, A., 2012. Recent advances in bone tissue engineering scaffolds. Trends Biotechnol. 30 (10), 546–554.

Burg, K.J. L., Porter, S., Kellam, J.F., 2000. Biomaterial developments for bone tissue engineering. Biomaterials 21, 2347–2359.

Bye, F.J., Bissoli, J., Black, L., Bullock, A.J., Puwanun, S., Moharamzadeh, K., Reilly, G.C., Ryan, A.J., Macneil, S., 2013. Development of bilayer and trilayer nanofibrous/microfibrous scaffolds for regenerative medicine. Biomater. Sci. 1, 942–951.

Carlberg, B., Axell, M.Z., Nannmark, U., Liu, J., Kuhn, H.G., 2009. Electrospun polyurethane scaffolds for proliferation and neuronal differentiation of human embryonic stem cells. Biomed. Mater. 4, 045004.

Clarke, D., Puppi, D., Detta, N., Ferrer, M.C. C., Crawford, A., Reilly, G., Chiellini, F., 2008. Electrospun polyurethane scaffolds for mechanical stimulation of cells in bone tissue engineering. Tissue Eng. Part A 14, 846 (pp.).

Croteau, S., Rauch, F., Silvestri, A., Hamdy, R.C., 1999. Bone morphogenetic proteins in orthopedics: From basic science to clinical practice. Orthopedics 22, 686–695.

Delaine-Smith, R., Macneil, S., Reilly, G., 2012. Matrix production and collagen structure are enhanced in two types of osteogenic progenitor cells by a simple fluid shear stress stimulus. Eur. Cells Mater. 24, 162–174.

Delaine-Smith, R.M., Green, N.H., Matcher, S.J., Macneil, S., Reilly, G.C., 2014. Monitoring fibrous scaffold guidance of three-dimensional collagen organisation using minimally-invasive second harmonic generation. PloS One 9, e89761.

Delaine-Smith, R.M., Reilly, G.C., 2011. The effects of mechanical loading on mesenchymal stem cell differentiation and matrix production. Vitam. Horm. 87, 417–480.

Demir, M.M., Yilgor, I., Yilgor, E., Erman, B., 2002. Electrospinning of polyurethane fibres. Polymer 24, 3303–3309.

Gogolewski, S., 2007. Structure-property relations and cytotoxicity of isosorbide-based biodegradable polyurethane scaffolds for tissue repair and regeneration. J. Biomed. Mater. Res. 85A, 456–465.

Gogolewski, S., Gorna, K., 2007. Biodegradable polyurethane cancellous bone graft substitutes in the treatment of iliac crest defects. J. Biomed. Mater. Res. Part A 80, 94–101.

Gorna, K., Gogolewski, S., 2003. Preparation, degradation, and calcification of biodegradable polyurethane foams for bone graft substitutes. J. Biomed. Mater. Res. Part A 67A, 813–827.

Gorna, K., Gogolewski, S., 2006. Biodegradable porous polyurethane scaffolds for tissue repair and regeneration. J. Biomed. Mater. Res. 79A, 128–138.

Grad, S., Kupcsik, L., Gorna, K., Gogolewski, S., Alini, M., 2003. The use of biodegradable polyurethane scaffolds for cartilage tissue engineering: potential and limitations. Biomaterials 24, 5163–5171.

Guelcher, S.A., 2008. Biodegradable polyurethanes: synthesis and applications in regenerative medicine. Tissue Eng. Part B: Rev. 14, 3–17.

Guelcher, S.A., Patel, V., Gallagher, K., Connolly, S., Didier, J.E., Doctor, J., Hollinger, J.O., 2004. Synthesis of polyurethane foam scaffolds for bone tissue engineering, Proc. AIChE, Annual meeting, Austin, Texas, 6261–6263 ISBN 0-8169-0965-2.

Heijkants, R., Van Tienen, T., de Groot, J., Pennings, A., Buma, P., Veth, R., Schouten, A., 2006. Preparation of a polyurethane scaffold for tissue engineering made by a combination of salt leaching and freeze-drying of dioxane. J. Mater. Sci. 41, 2423–2428.

Huang, Z.M., Zhang, Y.Z., Kotaki, M., Ramakrishna, S., 2003. A review on polymer nanofibers by electrospinning and their applications in nanocomposites. Compos. Sci. Technol. 63, 2223–2253.

Karlsson, C., Emanuelsson, K., Wessberg, F., Kajic, K., Axell, M.Z., Eriksson, P.S., Lindahl, A., Hyllner, J., Strehl, R., 2009. Human embryonic stem cell-derived mesenchymal progenitors—potential in regenerative medicine. Stem Cell Res. 3, 39–50.

Khan, A.S., Ahmed, Z., Edirisinghe, M.J., Wong, F.S. L., Rehman, I.U., 2008. Preparation and characterisation of a novel bioactive restorative composite based on covalently coupled polyurethane–nanohydroxyapatite fibres. Acta Biomater. 4, 1275–1287.

Khil, M.S., Cha, D.I., Kim, H.Y., Kim, I.S., Bhattarai, N., 2003. Electrospun nanofibrous polyurethane membrane as wound dressing. J. Biomed. Mater. Res. Part B—Appl. Biomater. 67B, 675–679.

Kucinska-Lipka, J., Gubanska, I., Janik, H., 2013. Gelatin-modified polyurethanes for soft tissue scaffold. Sci. World J. 2013 Article ID 450132, 12 pages, http://dx.doi.org/10.1155/2013/450132.

Lee, J.B., Jeong, S.I., Bae, M.S., Yang, D.H., Heo, D.N., Kim, C.H., Alsberg, E., Kwon, I.K., 2011. Highly porous electrospun nanofibers enhanced by ultrasonication for improved cellular infiltration. Tissue Eng. Part A 17, 2695–2702.

Leong, M.F., Chan, W.Y., Chian, K.S., Rasheed, M.Z., Anderson, J.M., 2010. Fabrication and in vitro and in vivo cell infiltration study of a bilayered cryogenic electrospun poly(D,L-lactide) scaffold. J. Biomed. Mater. Res. Part A 94A, 1141–1149.

Martin, T.P., 1996. Shells of atoms. Phys. Rep. 273, 199–241.

Martinez-Valencia, A., Carbajal-de La Torre, G., Torres-Sanchez, R., Tellez-Jurado, L., Esparza-Ponce, H., 2011. Production of

polyurethane/nano-hydroxyapatite hybrid materials and microstructural characterisation. Int. J. Phys. Sci. 6, 2731–2743.

Mcclure, M.J., Wolfe, P.S., Simpson, D.G., Sell, S.A., Bowlin, G.L., 2012. The use of air-flow impedance to control fiber deposition patterns during electrospinning. Biomaterials 33, 771–779.

Mcmahon, R.E., Qu, X., Jimenez-Vergara, A.C., Bashur, C.A., Guelcher, S.A., Goldstein, A.S., Hahn, M.S., 2011. Hydrogel–electrospun mesh composites for coronary artery bypass grafts. Tissue Eng. Part C: Methods 17, 451–461.

Mi, H.-Y., Palumbo, S., Jing, X., Turng, L.-S., Li, W.-J., Peng, X.-F, 2014. Thermoplastic polyurethane/hydroxyapatite electrospun scaffolds for bone tissue engineering: effects of polymer properties and particle size. J. Biomed. Mater. Res. Part B: Appl. Biomater., http://dx.doi.org/10.1002/jbm.b.33122.

Milleret, V., Simona, B., Neuenschwander, P., Hall, H., 2011. Tuning electrospinning parameters for production of 3D-fiber-fleeces with increased porosity for soft tissue engineering applications. Eur. Cell Mater. 21, 286–303.

Mo, C., Yuan, Z., Zhang, L., Xie, C, 1993. Infrared absorption spectra of nano-alumina. Nanostruct. Mater. 2, 47–54.

Nirmala, R., Kang, H.-S., EL-Newehy, M.H., Navamathavan, R., Park, H.-M., Kim, H.Y., 2011. Human osteoblast cytotoxicity study of electrospun polyurethane/calcium chloride ultrafine nanofibers. J. Nanosci. Nanotechnol. 11, 4749–4756.

Oprea, S., 2005. Effect of solvent interactions on the properties of polyurethane films. High Perform. Polym. 17, 163–173.

Patel, N., Best, S., Bonfield, W., Gibson, I., Hing, K., Damien, E., Revell, P., 2002. A comparative study on the in vivo behavior of hydroxyapatite and silicon substituted hydroxyapatite granules. J. Mater. Sci. Mater. Med. 13, 1199–1206.

Rehman, I., Bonfield, W., 1997. Characterisation of hydroxyapatite and carbonated apatite by photo acoustic FTIR spectroscopy. J. Mater. Sci. Mater. Med. 8, 1–4.

Rezwan, K., Chen, Q.Z., Blaker, J.J., Boccaccini, A.R., 2006. Biodegradable and bioactive porous polymer/inorganic composite scaffolds for bone tissue engineering. Biomaterials 27, 3413–3431.

Rosser, J., Bonewald, L.F., 2012. Studying Osteocyte Function Using the Cell Lines MLO-Y4 and MLO-A5. Bone Research Protocols. Humana Press, Springer, New York, NY.

Sittichockechaiwut, A., Scutt, A.M., Ryan, A.J., Bonewald, L.F., Reilly, G.C., 2009. Use of rapidly mineralising osteoblasts and short periods of mechanical loading to accelerate matrix maturation in 3D scaffolds. Bone 44, 822–829.

Sittichokechaiwut, A., Edwards, J., Scutt, A., Reilly, G., 2010. Short bouts of mechanical loading are as effective as dexamethasone at inducing matrix production by human bone marrow mesenchymal stem cell. Eur. Cell Mater. 20, 45–57.

Tsui, Y.K., Gogolewski, S., 2009. Microporous biodegradable polyurethane membranes for tissue engineering. J. Mater. Sci. Mater. Med. 20, 1729–1741.

Wannatong, L., Sirivat, A., Supaphol, P., 2004. Effects of solvents on electrospun polymeric fibres: preliminary study on polystyrene. Polym. Int. 53, 1851–1859.

Webster, T.J., Schadler, L.S., Siegel, R.W., Bizios, R., 2001. Mechanisms of enhanced osteoblast adhesion on nanophase alumina involve vitronectin. Tissue Eng. 7, 291–301.

Wen, J., Somorjai, G., Lim, F., Ward, R, 1997. XPS study of surface composition of a segmented polyurethane block copolymer modified by PDMS end groups and its blends with phenoxy. Macromolecules 30, 7206–7213.

Yoshii, T., Dumas, J.E., Okawa, A., Spengler, D.M., Guelcher, S.A., 2012. Synthesis, characterisation of calcium phosphates/polyurethane composites for weight-bearing implants. J. Biomed. Mater. Res. Part B: Appl. Biomater. 100B, 32–40.

Zdrahala, R.J., Zdrahala, I.J., 1999. Biomedical applications of polyurethanes: a review of past promises, present realities, and a vibrant future. J. Biomater. Appl. 14, 67–90.

Zhang, J., Doll, B.A., Beckman, E.J., Hollinger, J.O., 2003. A biodegradable polyurethane-ascorbic acid scaffold for bone tissue engineering. J. Biomed. Mater. Res.—Part A 67, 389–400.